Synthesis, Crystal Structures, and Catalytic Activity of Dicopper(II) Complexes with Dinucleating Tetraimidazole Ligands $[Cu_2(RO)(mbipl)](ClO_4)_2$ (R = Me, Et, 2-Pr; Hmbipl = 1,5-Bis[bis[(1-methyl-4-imidazolyl)methyl]amino]-3-pentanol) and $[Cu_2(MeO)(pbipl)](ClO_4)_2$ (Hpbipl = 1,5-Bis[bis[(1-isopropyl-4-imidazolyl)methyl]amino]-3-pentanol)

Masahito Kodera,*,† Norihisa Terasako,† Toshio Kita,† Yoshimitsu Tachi,† Koji Kano,† Mikio Yamazaki,‡ Masayuki Koikawa,§ and Tadashi Tokii§

Department of Molecular Science and Technology, Doshisha University, Kyotanabe, Kyoto 610-03, Japan, Rigaku-Denki, X-ray Laboratory, Akishima, Tokyo 196, Japan, and Department of Chemistry, Saga University, Saga 840, Japan

Received October 18, 1996[⊗]

Synthesis, crystal structures, and catalytic activity are reported for dinuclear copper(II) complexes of new dinucleating tetraimidazole ligands, 1,5-bis[bis[(1-methyl-4-imidazolyl)methyl]amino]-3-pentanol (Hmbipl) and 1,5-bis[bis[(1-isopropyl-4-imidazolyl)methyl]amino]-3-pentanol (Hpbipl). These ligands have been prepared by a reductive coupling of 1,5-diamino-3-pentanol with 4 equiv of 1-alkyl-4-formylimidazole (alkyl = methyl and isopropyl) by using sodium cyanoborohydride in quantitative yields. The ligand Hmbipl forms $[Cu_2(MeO)(mbipl)](ClO_4)_2$ (**1**) in MeOH. The methoxide bridge of **1** is easily exchanged with EtOH and 2-PrOH during recrystallization from such solvents, yielding ethoxide- and 2-propoxide-bridged complexes $[Cu_2(RO)(mbipl)](ClO_4)_2$ (R = Et, **2**; R = 2-Pr, **3**). The ligand Hpbipl forms $[Cu_2(MeO)(pbipl)](ClO_4)_2$ (**4**) in MeOH. Compounds **1**−**4** have been characterized by elemental analyses, FAB mass, electronic absorption, and IR spectra, magnetic susceptibilities, and cyclic voltammograms. Crystal structures of **2**·2MeCN and **3**·CH_2Cl_2 have been determined by X-ray analyses, showing that the coordination geometry about each copper ion in **2** and **3** is distorted trigonal bipyramidal. Compounds **1**−**4** catalyze the quantitative oxidation of 2,4-di-*tert*-butylphenol (DBP) to 3,3′,5,5′-tetra-*tert*-butyl-2,2′-dihydroxybiphenyl with H_2O_2. A hydroperoxodicopper(II) complex **5** which is generated from **4** as an active intermediate is detected by UV−vis spectroscopy. Compound **4** shows the highest activity among the present complexes because of its high reaction rate and high durability. Kinetic studies show that the reaction is first order with respect to both DBP and the catalyst. The second-order rate constant, k_2, is 5.3 M^{-1} s^{-1}. It seems that the bulky *N*-isopropyl groups enhance the catalytic activity of **4**.

Introduction

Oxidation catalyzed by copper complexes is of current interest.[1,2] In biological systems, phenols are oxidized to *o*-quinones by tyrosinase,[3] which is a monooxygenase having a dinuclear copper center as an active site similar to that of hemocyanin.[4,5] The dicopper center is coordinated by six histidyl imidazoles and binds dioxygen reversibly as a peroxide form. Although tyrosinase is the first discovered monooxygenase,[6] details of the dioxygen activation mechanism have not been elucidated completely.[7]

Biomimetic copper complexes are useful to deduce the mechanism of O_2 activation and the subsequent oxidation of substrates by tyrosinase.[8] Karlin et al. have synthesized peroxodicopper(II) complexes of tetrapyridyl hexa- and heptadentate ligands[9] and tripodal tetradentate ligands.[10] They have found that the peroxo complexes of the tetrapyridyl ligands oxidize 2,4-di-*tert*-butylphenol (DBP) to 3,3′,5,5′-tetra-*tert*-butyl-2,2′-dihydroxybiphenyl[9f] and also found that a hydro-

* To whom correspondence should be addressed.
† Doshisha University.
‡ Rigaku-Denki.
§ Saga University.
⊗ Abstract published in *Advance ACS Abstracts,* August 1, 1997.

(1) Kitajima, N.; Moro-oka, Y. *Chem. Rev.* **1994**, *94*, 737.
(2) Sorrell, T. N. *Tetrahedron* **1989**, *45*, 3.
(3) (a) Eickman, N. C.; Solomon, E. I.; Larrabee, J. A.; Spiro, T. G.; Lerch, K. *J. Am. Chem. Soc.* **1978**, *100*, 6529. (b) Himmelwright, R. S.; Eickman, N. C.; LuBien, C. D.; Lerch, K.; Solomon, E. I. *J. Am. Chem. Soc.* **1980**, *102*, 7339. (c) Wilcox, D. E.; Porras, A. G.; Hwang, Y. T.; Lerch, K.; Winkler, M. E.; Solomon, E. I. *J. Am. Chem. Soc.* **1985**, *107*, 4015.
(4) (a) Gaykema, W. P. J.; Hol, W. P. J.; Vereijken, J. M.; Soeter, M. M.; Bak, H. J.; Beintema, J. J. *Nature* **1984**, *303*, 23. (b) Ross, P. K.; Solomon, E. I. *J. Am. Chem. Soc.* **1991**, *113*, 3246. (c) Baldwin, M. J.; Root, D. E.; Pate, J. E.; Fujisawa, K.; Kitajima, N.; Solomon, E. I. *J. Am. Chem. Soc.* **1992**, *114*, 10421.
(5) Thamann, T. J.; Loehr, J. S.; Loehr, T. M. *J. Am. Chem. Soc.* **1977**, *99*, 4187.
(6) Mason, H. J.; Fowlks, W. B.; Peterson, E. W. *J. Am. Chem. Soc.* **1955**, *77*, 2914.
(7) Sánchez-Ferrer, A.; Rodríguez-López, J. N.; García-Cánovas, F.; García-Carmona, F. *Biochim. Biophys. Acta* **1995**, *1247*, 1.
(8) (a) Karlin, K. D.; Gultneh, Y. *Prog. Inorg. Chem.* **1987**, *35*, 219. (b) Tyeklár, Z.; Karlin, K. D. *Acc. Chem. Res.* **1989**, *22*, 241.
(9) (a) Karlin, K. D.; Hayes, J. C.; Gultneh, Y.; Cruse, R. W.; McKown, J. W.; Hutchinson, J. P.; Zubieta, J. *J. Am. Chem. Soc.* **1984**, *106*, 2121. (b) Karlin, K. D.; Cruse, R. W.; Gultneh, Y. *J. Chem. Soc., Chem. Commun.* **1987**, 599. (c) Karlin, K. D.; Cohen, B. I.; Jacobson, R. R.; Zubieta, J. *J. Am. Chem. Soc.* **1987**, *109*, 6194. (d) Karlin, K. D.; Haka, M. S.; Cruse, R. W.; Meyer, G. J.; Farooq, A.; Gultneh, Y.; Zubieta, J. *J. Am. Chem. Soc.* **1988**, *110*, 1196. (e) Cruse, R. W.; Kaderli, S.; Meyer, C. J.; Zuberbühler, A. D.; Karlin, K. D. *J. Am. Chem. Soc.* **1988**, *110*, 5020. (f) Paul, P. P.; Tyeklár, Z.; Jacobson, R. R.; Karlin, K. D. *J. Am. Chem. Soc.* **1991**, *113*, 5322. (g) Karlin, K. D.; Tyeklár, Z.; Farooq, A.; Haka, M. S.; Ghosh, P.; Cruse, R. W.; Gultneh, Y.; Hayes, J. C.; Toscano, P. J.; Zubieta, J. *Inorg. Chem.* **1992**, *31*, 1436. (h) Nasir, M. S.; Cohen, B. I.; Karlin, K. D. *J. Am. Chem. Soc.* **1992**, *114*, 2482. (i) Sanyal, I.; Murthy, N. N.; Karlin, K. D. *Inorg. Chem.* **1993**, *32*, 5330. (j) Karlin, K. D.; Nasir, M. S.; Cohen, B. I.; Cruse, R. W.; Kaderli, S.; Zuberbühler, A. D. *J. Am. Chem. Soc.* **1994**, *116*, 1324.

S0020-1669(96)01267-0 CCC: $14.00 © 1997 American Chemical Society

peroxodicopper(II) complex is generated by protonation of the peroxo complex and oxidizes triphenylphosphine quantitatively.[9b] Itoh et al. found an interesting ligand hydroxylation *via* a peroxodicopper(II) complex with a tridentate ligand, *N*,*N*-bis-[2-(2-pyridyl)ethyl]-2-phenylethylamine.[11] Valentine et al. reported catalytic epoxidations of olefines with iodosobenzene as an oxidant and suggested that a high-valent oxocopper species might be involved.[12] Kitajima et al. have prepared thermally stable μ-η^2:η^2-peroxodicopper(II) complexes with sterically hindered tris(pyrazolyl)borate ligands.[13] Some of these peroxo complexes oxidize phenols to coupling products.[13c] A similar peroxodicopper(II) complex of *N*,*N*,*N*-triisopropyltriazacyclononane has been prepared by Tolman et al.[14] They observed H−D exchange at the methine groups of the ligand in deuterium solvent and proposed a new mechanism of the dioxygen activation *via* a homolytic scission of the O−O bond in the peroxo complex.[15]

In spite of the biological importance of imidazole ligands in the copper proteins, only few dicopper complexes of polyimidazole ligands have been known.[16] We have prepared new tetraimidazolyl heptadentate ligands, 1,5-bis[bis[(1-methyl-4-imidazolyl)methyl]amino]-3-pentanol (Hmbipl) and 1,5-bis[bis-[(1-isopropyl-4-imidazolyl)methyl]amino]-3-pentanol (Hpbipl), to prepare functional models of tyrosinase. The dicopper(II) complexes of these ligands catalyze the oxidation of phenol efficiently. The dicopper complex of Hpbipl, **4**, shows the highest activity, though bulky alkyl groups are known to stabilize reactive intermediates and metal dioxygen complexes by lowering the reactivities.[13b,27] The effect of the isopropyl groups on the catalytic activity in **4** will be discussed.

Experimental Section

All ordinary reagents and solvents were purchased and used as received unless otherwise noted. 4-Formylimidazole and 1,5-diamino-3-pentanol were prepared according to the previous work.[16a] Absolute MeOH and EtOH were obtained by distillation over Mg. MeCN and CH_2Cl_2 were dried over P_2O_5 and distilled. DMF was dried over anhydrous barium oxide in the dark and then distillated under reduced pressure.

Measurements. Elemental analyses (C, H, N) were carried out at the Elemental Analysis Service Center of Kyoto University. The amounts of copper were determined on a Shimazu AA-610 atomic absorption/flame emission spectrophotometer. ^{1}H and ^{13}C NMR spectra in $CDCl_3$ and D_2O were recorded on a JEOL JMN-A 400 spectrometer using Me_4Si and sodium (trimethylsilyl)propionate-d_4 (TSP) as internal standards. Assignment of all ^{13}C signals was ascertained by C−H COSY spectra. Infrared (IR) spectra were taken on a Shimadzu IR-400 spectrometer with KBr disks. UV−vis absorption spectra were recorded on a Hitachi U-3210 spectrophotometer and on a Shimadzu UV-3100 spectrophotometer in MeOH for the ligands Hmbipl and Hpbipl and in MeCN for compounds **1**−**4**. Fast atom bombardment (FAB) mass spectra were obtained on a JEOL JMS-DX 300 spectrometer using *m*-nitrobenzyl alcohol (NBA) as a matrix. Magnetic susceptibilities were measured in the range 80−300 K on a Faraday balance. The apparatus was calibrated with $[Ni(en)_3][S_2O_3]$.[17] The data for the diamagnetism of the constituent atoms were corrected by the use of Pascal's constants.[18] Cyclic voltammograms (CV) were recorded on a BAS CV-50W voltammetric analyzer. The CV measurements were carried out in MeCN (ca. 1×10^{-3} mol dm^{-3}) using $(Bu_4N)ClO_4$ (TBAP) as a supporting electrolyte. A three-electrode cell composed of a glassy-carbon working electrode, a platinum-wire auxiliary electrode, and a referencial electrode, Ag/Ag^+ (TBAP/MeCN), was used. GLC analysis of the oxidized products was carried out by using a Shimadzu GC-8A gas chromatograph using a thermon-1000 + H_3PO_4 column (3 mm diameter × 0.8 m, at gradient temperature 80−240 °C for 20 min, He carrier 0.5 kg/cm^2).

Preparations. 1-Methyl-4-formylimidazole. In 300 mL of a two necked flask was placed 2.08 g (52.1 mmol) of NaH (60% oil dispersion), which was washed with *n*-hexane (3 × 20 mL) and dried *in vacuo*. To the flask was added 70 mL of dry DMF, which was degassed by three cycles of evacuation and refilling with Ar. After the mixture was cooled to 0 °C, 5 g (52.1 mmol) of 4-formylimidazole was added. At that time, H_2 gas was vigorously evolved. After the gas evolution was completed, 8.3 g (58.5 mmol) of methyl iodide was added to the mixture under Ar at 0 °C. The mixture was stirred at room temperature for 3 h. The reaction was monitored by TLC. After the reaction was completed, the reaction mixture was concentrated under reduced pressure. The residue was dissolved in 100 mL of $CHCl_3$ and washed with 50 mL of distilled water. The aqueous layer was extracted with $CHCl_3$ (2 × 100 mL). The $CHCl_3$ layer and the extracts were combined and dried over anhydrous Na_2SO_3. The $CHCl_3$ solution was concentrated to dryness. The residue was purified by a silica gel column chromatography ($CHCl_3$−MeOH, 10:1, v/v), giving 1-methyl-4-formylimidazole (1.72 g, 30%): Mp 35−37 °C. Anal. Calcd for $C_5H_6N_2O$: C, 54.54; H, 5.49; N, 25.44. Found: C, 54.51; H, 5.48; N, 25.73. IR (KBr disk) (ν_{max}/cm^{-1}): 3100 and 3080 (aromatic CH), 2970 (aliphatic CH), 2800 (aldehyde CH), and 1665 (carbonyl CO). NMR (in $CDCl_3$): ^{1}H, δ 3.96 (3H, s, CH_3), 7.63 (1H, s, 5-H of imidazole), 7.77 (1H, s, 2-H of imidazole), and 9.76 (1H, s, CH of aldehyde); ^{13}C, δ 34.0 (CH_3), 125.64 (5-C of imidazole ring), 139.5 (2-C of imidazole ring), 142.5 (4-C of imidazole ring), and 186.1 (C═O of aldehyde). The 3-methylated isomer was separated by the column chromatography (1.55 g, 27%).

1-Isopropyl-4-formylimidazole. This compound was prepared by the same method as above except for using isopropyl iodide in place of methyl iodide (5.2 g, 72%): Mp 52−54 °C. Anal. Calcd for $C_7H_{10}N_2O$: C, 60.85; H, 7.30; N, 20.27. Found: C, 60.62; H, 7.31; N, 20.07. IR (KBr disk) (ν_{max}/cm^{-1}): 3100 and 3080 (aromatic CH), 2970 and 2930 (aliphatic CH), 2800 (aldehyde CH), and 1665 (carbonyl C═O). NMR (in $CDCl_3$): ^{1}H, δ 1.54 (6H, s, CH_3), 4.45(1H, septet, CH of isopropyl), 7.34 (1H, s, 5-H of imidazole), 7.71 (1H, s, 2-H of imidazole), and 9.87 (1H, s, CH of aldehyde); ^{13}C, δ 23.65 (CH_3 of isopropyl), 50.15 (CH of isopropyl), 122.2 (5-C of imidazole ring), 137.1 (2-C of imidazole ring), 142.4 (4-C of imidazole ring), and 186.4 (C═O of aldehyde).

(10) (a) Cruse, R. W.; Kaderli, S.; Karlin, K. D.; Zuberbühler, A. D. *J. Am. Chem. Soc.* **1988**, *110*, 6882. (b) Jacobson, R. R.; Tyeklár, Z.; Farooq, A.; Karlin, K. D.; Liu, S.; Zubieta, J. *J. Am. Chem. Soc.* **1988**, *110*, 3690. (c) Karlin, K. D.; Wei, N.; Jun, B.; Kaderli, S.; Zuberbühler, A. D. *J. Am. Chem. Soc.* **1991**, *113*, 5868. (d) Tyeklár, Z.; Jacobson, R. R.; Wei, N.; Narasimha, N.; J. Zubieta, M.; Karlin, K. D. *J. Am. Chem. Soc.* **1993**, *115*, 2677. (e) Karlin, K. D.; Wei, N.; Jung, B.; Kaderli, S.; Niklaus, P.; Zuberbühler, A. D. *J. Am. Chem. Soc.* **1993**, *115*, 9506.

(11) Itoh, S.; Kondo, T.; Komatsu, M.; Ohshiro, Y.; Li, C.; Kanehisa, N.; Kai, Y.; Fukuzumi, S. *J. Am. Chem. Soc.* **1995**, *116*, 4717.

(12) Franklin, C. C.; Vanatta, R. B.; Tai, A. F.; Valentine, S. J. *J. Am. Chem. Soc.* **1984**, *106*, 814.

(13) (a) Kitajima, N.; Fukui, H.; Moro-oka, Y. *J. Chem. Soc., Chem. Commun.* **1988**, 485. (b) Kitajima, N.; Fujisawa, K.; Moro-oka, Y.; Toriumi, K. *J. Am. Chem. Soc.* **1989**, *111*, 8975. (c) Kitajima, N.; Koda, T.; Iwata, Y.; Moro-oka, Y. *J. Am. Chem. Soc.* **1990**, *112*, 8833. (d) Kitajima, N.; Fujisawa, K.; Fujimoto, C.; Moro-oka, Y.; Hashimoto, S.; Kitagawa, T.; Toriumi, K.; Tatsumi, K.; Nakamura, A. *J. Am. Chem. Soc.* **1992**, *114*, 1277.

(14) Mahapatra, S.; Halfen, J. A.; Wilkinson, E. C.; Que, L., Jr.; Tolman, W. B. *J. Am. Chem. Soc.* **1994**, *116*, 9785.

(15) Halfen, J. A.; Mahapatra, S.; Wilkinson, E. C.; Kaderli, S.; Young, V. J., Jr.; Que, L., Jr.; Zuberbühler, A. D.; Tolman, W. B. *Science* **1996**, *271*, 1397.

(16) (a) Kodera, M.; Koura, N.; Hosohara, S.; Nishimura, M.; Ohba, M.; Okawa, H.; Kida, S. *Inorg. Chim. Acta* **1993**, *214*, 97. (b) Sorrell, T. N.; Borovik, A. S. *J. Am. Chem. Soc.* **1987**, *109*, 4255. (c) Sorrell, T. N.; Vankai, V. A.; Garrity, M. L. *Inorg. Chem.* **1991**, *30*, 207. (d) Sorrell, T. N.; Garrity, M. L. *Inorg. Chem.* **1991**, *30*, 210. (e) Tolman, W. B.; Rardin, R. L.; Lippard, S. J. *J. Am. Chem. Soc.* **1989**, *111*, 4532. (f) Oberhausen, K. J.; Richardson, J. F.; Buchanan, R. M.; McCusker, J. K.; Hendrickson, D. N.; Latour, J.-M. *Inorg. Chem.* **1991**, *30*, 1357. (g) Nei, H.; Aubin, S. M. J.; Mashuta, M. S.; Porter, R. A.; Richardson, J. F.; Hendrickson, D. N.; Buchanan, R. M. *Inorg. Chem.* **1996**, *35*, 3325. (h) Lynch, W. E.; Kurtz, D. M., Jr.; Wang, S.; Scott, R. A. *J. Am. Chem. Soc.* **1994**, *116*, 11030.

(17) Curtis, N. F. *J. Chem. Soc.* **1961**, 3147.

(18) Mulay, L. N. *Theory and Applications of Molecular Paramagnetism*; Wiley: New York, 1976; p 491.

1,5-Bis[bis[(1-methyl-4-imidazolyl)methyl]amino]-3-pentanol−6-Hydrogen Chloride−4-Water (Hmbipl·6HCl·4H$_2$O). 1-Methyl-4-formylimidazole (1.48 g; 13.45 mmol) and 0.642 g (3.36 mmol) of 1,5-diamino-3-pentanol dihydrochloride were dissolved in 25 mL of absolute MeOH. The solution was cooled to 0 °C and degassed by three cycles of evacuation and refilling with Ar. Then 1.0 g (15.87 mmol) of sodium cyanoborohydride was added to this solution at 0 °C under Ar. The mixture was stirred at 0 °C for 2 h and then at room temperature for 12 h. The white solid generated during the reaction was filtered off. To the filtrate was added 2 mL of concentrated HCl to decompose the remaining cyanoborohydride. The resultant acidic solution was concentrated to dryness. To the residue was added 20 mL of absolute MeOH, and insoluble materials were removed by filtration. To the filtrate was added 0.5 mL of concentrated HCl. This cycle was repeated until no more insoluble solids were generated. After this cycle, the oily residue was dissolved in 5 mL of absolute EtOH. To the solution was added 20 mL of acetone to precipitate the HCl salt of Hmbipl as a white solid, which was collected by filtration, washed with acetone, and dried *in vacuo* (2.50 g, 95%). The product is hygroscopic: Mp 128 °C (dec). Anal. Calcd for $C_{25}H_{52}Cl_6N_{10}O_5$: C, 38.23; H, 6.67; N, 17.83; Cl, 27.08. Found: C, 38.40; H, 6.75; N, 17.86; Cl, 27.83. UV−vis absorption data (in MeOH) [λ_{max}/nm (ϵ_{max}/dm^3 mol^{-1} cm^{-1})]: 210 (21 300). IR (KBr disk) (ν_{max}/cm^{-1}): 3400 (OH), 3100 (aromatic CH), 2970 (aliphatic CH), and 1615 (imidazole ring). NMR (D_2O): ^{1}H, δ 1.93−2.18 (4H, m, 2,4-CH_2 of alkyl chain), 3.24−3.40 (4H, m, 1,5-CH_2 of alkyl chain), 3.75−3.86 (1H, m, 3-CH of alkyl chain), 3.96 (12H, s, CH_3), 4.57 (8H, s, CH_2), 7.83 (4H, s, 5-H of imidazole), and 8.84 (4H, s, 2-H of imidazole); ^{13}C, δ 31.48 (2,4-CH_2 of alkyl chain), 36.65 (CH_3), 46.97 (CH_2), 50.71 (1,5-CH_2 of alkyl chain), 67.40 (3-CH of alkyl chain), 122.98 (4-C of imidazole ring), 126.65 (5-C of imidazole ring), and 138.03 (2-C of imidazole ring). FAB mass data: *m*/*z* 495 [M − 6HCl + H]$^+$.

1,5-Bis[bis[(1-isopropyl-4-imidazolyl)methyl]amino]-3-pentanol−6-Hydrogen Chloride−5-Water (Hpbipl·6HCl·5H$_2$O). 1,5-Diamino-3-pentanol dihydrochloride (307 mg,1.61 mmol) and 950 mg (6.88 mmol) of 1-isopropyl-4-formylimidazole were dissolved in 20 mL of absolute MeOH, and the solution was deaerated as mentioned above. To the solution was added 455 mg (7.22 mmol) of sodium cyanoborohydride under Ar. The mixture was stirred at room temperature for 20 h. After the reaction mixture was worked up as mentioned above, the product was isolated as white solid (1.1 g, 81%). The product is hygroscopic: Mp 154 °C (dec). Anal. Calcd for $C_{33}H_{70}Cl_6N_{10}O_6$: C, 43.29; H, 7.71; N, 16.29; Cl, 23.23. Found: C, 43.51; H, 7.77; N, 15.35; Cl, 24.01. UV−vis absorption data (MeOH) [λ_{max}/nm (ϵ_{max}/dm^3 mol^{-1} cm^{-1})]: 210 (21 500). IR (KBr disk) (ν_{max}/cm^{-1}): 3350 (OH), 3100 (aromatic CH), 2970 (aliphatic CH), and 1615 (imidazole ring). NMR (D_2O): ^{1}H, δ 1.38 (24H, d, CH_3 of isopropyl), 1.77−2.00 (4H, broad, 2,4-CH_2 of alkyl chain), 3.15−3.20 (4H, broad, 1,5-CH_2 of alkyl chain), 3.59−3.63 (1H, broad, 3-CH of alkyl chain), 4.46 (8H, s, CH_2), 4.54 (4H, septet, CH of isopropyl), 7.85 (4H, s, 5′-H of imidazole), and 8.78 (4H, s, 2′-H of imidazole); ^{13}C, δ 22.67 (CH_3 of isopropyl), 31.69 (2,4-CH_2 of alkyl chain), 47.24 (CH_2), 50.69 (1,5-CH_2 of alkyl chain), 54.27 (CH of isopropyl), 67.40 (3-CH of alkyl chain), 123.51 (5-C of imidazole ring), 123.80 (4-C of imidazole ring), and 135.91 (2-C of imidazole ring). FAB mass data: *m*/*z* 607 [M − 6HCl + H]$^+$.

[Cu$_2$(MeO)(mbipl)](ClO$_4$)$_2$ (1). Hmbipl·6HCl·4H$_2$O (350 mg, 0.45 mmol) was dissolved in 10 mL of absolute MeOH, and 370 mg (1.00 mmol) of Cu(ClO$_4$)$_2$·6H$_2$O was added to the solution, yielding the dark blue solution. The solution was neutralized by NaOH, to afford the green precipitates. The solid was collected by filtration, washed with a small amount of MeOH, and dried *in vacuo*. The green solid was recrystallized from Et$_2$O−MeCN to give greenish prismatic crystals (270 mg, 70%). Anal. Calcd for $C_{26}H_{42}Cl_2Cu_2N_{10}O_{11}$: C, 35.95; H, 4.87; N, 16.12; Cu, 14.63. Found: C, 35.86; H, 4.66; N, 16.48; Cu, 14.95. UV−vis absorption data (in MeCN) [λ_{max}/nm (ϵ_{max}/dm^3 mol^{-1} cm^{-1})]: 269 (6770), 375 (sh), and 878 (226). IR (KBr disk) (ν_{max}/cm^{-1}): 3120 (aromatic CH), 2920 and 2850 (aliphatic CH), 1518, 1450, and 1420 (imidazole ring), and 1165, 1145, and 1100 (perchlorate ion). FAB mass data: *m*/*z* 870 [M − CH_3O − ClO_4 + NBA − H]$^+$, 771 [M − CH_3O − 2ClO_4 + NBA − H]$^+$, 719 [M − CH_3O − ClO_4 + H]$^+$, 619 [M − CH_3O − 2ClO_4]$^+$, and 557 [M − CH_3O − Cu − 2ClO_4 + H]$^+$.

[Cu$_2$(EtO)(mbipl)](ClO$_4$)$_2$ (2). The recystallization of **1** (60 mg) from MeCN−EtOH gave green crystals of **2** (50 mg, 82%). Anal. Calcd for $C_{27}H_{42}Cl_2Cu_2N_{10}O_{10}$: C, 37.50; H, 4.90; N, 16.20; Cu, 14.70. Found: C, 37.40; H, 4.93; N, 16.52; Cu, 14.26. UV−vis absorption data (MeCN) [λ_{max}/nm (ϵ_{max}/dm^3 mol^{-1} cm^{-1})]: 268 (5930), 375 (sh), and 876 (225). IR (KBr disk) (ν_{max}/cm^{-1}): 3120 (aromatic CH), 2920 and 2850 (aliphatic CH), 1518, 1450, and 1420 (imidazole ring), and 1165, 1145, and 1100 (perchlorate ion). FAB mass data: *m*/*z* 870 [M − C_2H_5O − ClO_4 + NBA − H]$^+$, 771 [M − C_2H_5O − 2ClO_4 + NBA − H]$^+$, 719 [M − C_2H_5O − ClO_4 + H]$^+$, 619 [M − C_2H_5O − 2ClO_4]$^+$, and 557 [M − C_2H_5O − Cu − 2ClO_4 + H]$^+$.

[Cu$_2$(2-PrO)(mbipl)](ClO$_4$)$_2$ (3). The recrystallization of **1** (60 mg) from MeCN−CH_2Cl_2−2-PrOH gave green crystals of **3** (55 mg, 89%). Anal. Calcd for $C_{31}H_{52}Cl_2Cu_2N_{10}O_{11}$: C, 39.66; H, 5.58; N, 14.92; Cu, 13.57. Found: C, 39.41; H, 5.57; N, 15.13; Cu, 13.80. UV−vis absorption data (MeCN) [λ_{max}/nm (ϵ_{max}/dm^3 mol^{-1} cm^{-1})]: 268 (6200), 375 (sh), and 875 (208). IR (KBr disk) (ν_{max}/cm^{-1}): 3100 (aromatic CH), 2900 and 2840 (aliphatic CH), 1510, 1445, and 1415 (imidazole ring), and 1160 and 1100 (perchlorate ion). FAB mass data: *m*/*z* 870 [M − C_3H_7O − ClO_4 + NBA − H]$^+$, 771 [M − C_3H_7O − 2ClO_4 + NBA − H]$^+$, 719 [M − C_3H_7O − ClO_4 + H]$^+$, 619 [M − C_3H_7O − 2ClO_4]$^+$, and 557 [M − C_3H_7O − Cu − 2ClO_4 + H]$^+$.

[Cu$_2$(MeO)(pbipl)](ClO$_4$)$_2$ (4). Hpbipl·6HCl·5H$_2$O (230 mg, 0.25 mmol) was dissolved in 5 mL of absolute MeOH, and 200 mg (0.54 mmol) of Cu(ClO$_4$)$_2$·6H$_2$O was added to the solution. When the solution was neutralized by NaOH, the color of the solution turned green. The green solid was precipitated gradually. The solid was collected by filtration and washed with MeOH. The solid was recrystallized from CH_2Cl_2−MeOH−dioxane to give green crystals (125 mg, 52%). Anal. Calcd for $C_{34}H_{56}Cl_2Cu_2N_{10}O_{10}$: C, 42.41; H, 5.86; N, 14.55; Cu, 13.20. Found: C, 41.85; H, 5.86; N, 14.61; Cu, 12.80. UV−vis absorption data (MeCN) [λ_{max}/nm (ϵ_{max}/dm^3 mol^{-1} cm^{-1})]: 267 (6370), 370 (sh), and 862 (228). IR (KBr disk) (ν_{max}/cm^{-1}): 3100 (aromatic CH), 2950, 2900, and 2850 (aliphatic CH), 1500, 1450, and 1415 (imidazole ring), and 1175, 1145, and 1100 (perchlorate ion). FAB mass data: *m*/*z* 1083 [M − CH_3O + NBA + H]$^+$, 982 [M − CH_3O − ClO_4 + NBA − H]$^+$, 883 [M − CH_3O − 2ClO_4 + NBA − H]$^+$, 831 [M − CH_3O − ClO_4 + H]$^+$, 731 [M − CH_3O − 2ClO_4]$^+$, and 669 [M − CH_3O − Cu − 2ClO_4 + H]$^+$.

Structure Determinations of Single Crystals. The structure of **2** was determined on a Rigaku AFC5R diffractometer with graphite-monochromated Cu Kα radiation and a 12 kW rotating anode generator at 298 ± 1 K. The structure of **3** was ascertained on a Rigaku AFC7R diffractometer with graphite monochromated Mo Kα radiation and a 12 kW rotating anode generator at 293 ± 1 K. Total numbers of reflections 6733 and 10 099 were collected for **2** and **3**, respectively. The intensities of three representative reflections were measured after every 150 reflections. All three structures were solved by direct methods (SHELEXS 86)[19] and expanded using Fourier techniques. The function minimized was $\sum w(|F_o| - |F_c|)^2$ with $w = 1/\sigma^2(F_o)$. The neutral atom scattering factors were taken from Cromer and Waber.[20] Anomalous dispersion effects were included in F_c,[21] the values for $\Delta f'$ and $\Delta f''$ being taken from ref 22 and those for the mass-attenuation coefficients from ref 23. All calculations were performed using the teXsan crystallographic software pakage.[24] Key facets of the three structure determinations are given in Table 1. The positional parameters of non-hydrogen atoms of **3**·CH_2Cl_2 are given in Table 2. The experimental details of the X-ray analyses are given in the Supporting Information.

Oxidation of 2,4-Di-*tert*-butylphenol (DBP). To a 30 mL pear-shaped flask was added an MeCN−CH_2Cl_2 (0.2 mL/3 mL) solution containing 0.005 mmol of the dicopper complex, 0.25 mmol of DBP, and 60 μL of nitrobenzene as an internal standard for GLC analysis.

(19) Sheldrick, G. M. *Acta Crystallogr., Sect. A* **1990**, *46*, 467.
(20) Cromer, D. T.; Waber, J. T. *International Tables for X-Ray Crystallography*; Kynoch Press: Birmingham, U.K., 1974; Vol. 4.
(21) Ibers, J. A.; Hamilton, W. C. *Acta Crystllogr.* **1964**, *17*, 781.
(22) Creagh, D. C.; McAuley, W. J. *International Tables for X-Ray Crystallography*; Kluwer: Boston, MA 1992; p 219.
(23) Creagh, D. C.; Hubbell, H. H. *International Tables for X-Ray Crystallography*; Kluwer: Boston, MA, 1992; p 200.
(24) Single crystal structure analysis software, version 1.6, Molecular Structure Corp., The Woodlands, TX 77381, 1993.

Table 1. Crystallographic Data for **2**·2MeCN and **3**·CH_2Cl_2

	2·2MeCN	**3**·CH_2Cl_2.
formula	$C_{31}H_{45}Cl_2Cu_2N_{12}O_{10}$	$C_{29}H_{46}Cl_4Cu_2N_{10}O_{10}$
fw	943.77	963.65
cryst system	monoclinic	monoclinic
space group	$P2_1/n$ (No. 14)	$C2/c$ (No. 15)
a/Å	10.689(1)	27.619(8)
b/Å	24.456(3)	10.467(8)
c/Å	16.228(2)	28.971(4)
β/deg	90.54(1)	102.68(2)
V/Å^3	4243.3(8)	8170(6)
Z	4	8
T/°C	25	20
D_c/g cm^{-3}	1.477	1.567
radiation/Å	Cu Kα ($\lambda = 1.541\ 78$)	Mo Kα ($\lambda = 0.710\ 69$)
μ/cm^{-1}	29.56	13.66
R, R_w[a]	0.073, 0.081	0.065, 0.089
GOF index	3.06	2.73

[a] $R = \sum||F_o| - |F_c||/\sum|F_o|$. $R_w = [\sum w(|F_o| - |F_c|)^2/\sum w(F_o)^2]^{1/2}$, where $w = 1/\sigma^2(F_o)$.

The reaction started upon addition of 30 μL of aqueous H_2O_2 (30%). From the reaction mixture, 0.05 mL aliquots were taken every 1 min and immediately added to Et_2O (2 mL) to terminate the reaction by dilution. The Et_2O solution was analyzed by GLC. DBP and the coupling product, 3,3′,5,5′-tetra-*tert*-butyl-2,2′-dihydroxybiphenyl (retention times of these compounds were 13.3 and 18.1 min, respectively; GLC conditions as described above), were determined quantitatively on the basis of added nitrobenzene standard.

The decomposition of the dicopper complex during treatment was monitored by electronic absorption spectrophotometry.

Results and Discussion

Synthesis of Ligands. In a previous work, we showed that tetraimidazole heptadentate ligand 1,5-bis[bis[imidazolylmethyl]-amino]-3-pentanol (Hbipl) is obtained by one-pot reaction of 1,5-diamino-3-pentanol with 4-formylimidazole in the presence of sodium cyanoborohydride and that Hbipl forms dicopper(II) and diiron(III) complexes.[16a] These complexes, however, did not yield single crystals suitable for X-ray structure analysis. This is due to low solubility of the complex in organic solvents as well as the problem of a dissociable NH hydrogen of the pendant imidazole ring in Hbipl. The *N*-anion generated by deprotonation can be bound to another metal ion, resulting in the formation of insoluble polymer complexes. In order to solve these problems, we have tried to block the free NH group by *N*-alkylation.

The synthetic route of the *N*-alkyl-substituted tetraimidazole dinucleating ligands, Hmbipl and Hpbipl, is shown in Scheme 1. 4-Formylimidazole was treated with 1 equiv of NaH, and the resultant *N*-anion was reacted with alkyl halide. The *N*-alkylation is expected to occur at the 1- and 3-nitrogens of the imidazole ring. In the case of methylation, both the 1- and 3-methyl isomers were obtained in a 1:1 ratio. This causes the low yield of 1-methyl-4-formylimidazole (ca. 30%). On the other hand, *N*-isopropylation by the same method occurred at the sterically less hindered site to give the 1-isopropyl isomer predominantly, leading to the relatively high yield (ca. 70%) of 1-isopropyl-4-formylimidazole. The dinucleating ligands Hmbipl and Hpbipl have been prepared quantitatively *via* a reductive condensation of 1,5-diamino-3-pentanol with 4 equiv of 1-alkyl-4-formylimidazole (alkyl = methyl and isopropyl), respectively. These imidazole compounds and the ligands were characterized by means of NMR spectroscopy. The ^{13}C NMR chemical shifts of the imidazole ring carbon atoms of Hmbipl are similar to those of Hbipl. This suggests that *N*-methylation gives only weak electronic effect on the imidazole ring. The ^{13}C NMR signals of the 2- and 5-carbon atoms in Hpbipl shift to higher magnetic fields by ca. 3 ppm compared with those in Hmbipl. This may be due to a steric effect of the bulky *N*-isopropyl groups in Hpbipl. Interestingly the 4-carbon atom does not show such a shift in the ^{13}C NMR spectra. The ^{13}C and ^1H NMR signals of the spacer group which connects the two tridentate sites of the ligand are almost identical between the three ligands, Hbipl, Hmbipl, and Hpbipl, indicating that *N*-alkylation does not impart significant electronic and steric effects to the spacer group.

Table 2. Positional and Thermal (Å^2) Parameters for **3**·CH_2Cl_2

atom	x	y	z	B_{eq}[a]
Cu(1)	0.18070(4)	0.7739(1)	0.16077(4)	3.49(3)
Cu(2)	0.12638(4)	0.7785(1)	0.06196(4)	3.56(3)
Cl(1)	0.0236(1)	0.2129(4)	0.1604(1)	6.12(9)
Cl(2)	0.3138(2)	0.1859(4)	0.0772(2)	8.5(1)
Cl(3)	0.4716(4)	0.113(1)	0.1199(5)	29.9(6)
Cl(4)	0.5323(4)	0.198(1)	0.1933(4)	27.3(5)
O(1)	0.1589(2)	0.6491(6)	0.1096(2)	3.7(2)
O(2)	0.1511(2)	0.8957(6)	0.1130(2)	3.6(2)
O(3)	0.0336(5)	0.237(2)	0.1174(4)	15.3(5)
O(4)	−0.0200(5)	0.261(2)	0.1597(7)	19.5(7)
O(5)	0.0570(6)	0.261(2)	0.1954(5)	18.1(6)
O(6)	0.01835(3)	0.079(1)	0.1657(4)	11.0(4)
O(7)	0.2905(8)	0.092(2)	0.0532(7)	22.7(9)
O(8)	0.3340(7)	0.267(2)	0.061(1)	31(1)
O(9)	0.2836(8)	0.229(2)	0.1030(9)	24(1)
O(10)	0.3543(9)	0.128(3)	0.1088(7)	25(1)
N(1)	0.2061(3)	0.6307(8)	0.2106(3)	4.3(2)
N(2)	0.1530(3)	0.8492(8)	0.2146(3)	4.0(2)
N(3)	0.1089(4)	0.9134(9)	0.2644(3)	5.3(3)
N(4)	0.2620(3)	0.8046(8)	0.1702(3)	4.0(2)
N(5)	0.3423(3)	0.8502(10)	0.1898(3)	4.6(2)
N(6)	0.0935(4)	0.6409(8)	0.0118(3)	4.7(2)
N(7)	0.1675(3)	0.8151(8)	0.0104(3)	4.5(2)
N(8)	0.2077(4)	0.866(1)	−0.0442(3)	5.5(3)
N(9)	0.0556(3)	0.8438(8)	0.0479(3)	4.2(2)
N(10)	−0.0208(3)	0.8936(9)	0.0465(3)	5.1(3)
C(1)	0.1718(5)	0.520(1)	0.2053(4)	5.3(3)
C(2)	0.1585(4)	0.460(1)	0.1573(4)	5.1(3)
C(3)	0.1298(4)	0.5415(10)	0.1178(4)	4.5(3)
C(4)	0.1137(5)	0.4624(10)	0.0731(4)	5.6(3)
C(5)	0.0770(4)	0.5255(10)	0.0335(4)	5.0(3)
C(6)	0.2103(4)	0.693(1)	0.2580(4)	4.9(3)
C(7)	0.1689(4)	0.785(1)	0.2565(4)	4.6(3)
C(8)	0.1405(5)	0.825(1)	0.2872(4)	5.6(3)
C(9)	0.1165(4)	0.925(1)	0.2207(4)	4.5(3)
C(10)	0.0710(5)	0.978(1)	0.2842(5)	7.0(4)
C(11)	0.2576(4)	0.593(1)	0.2058(4)	5.2(3)
C(12)	0.2874(4)	0.706(1)	0.1975(4)	4.3(3)
C(13)	0.3361(4)	0.735(1)	0.2100(4)	5.6(3)
C(14)	0.2970(4)	0.888(1)	0.1665(4)	4.1(3)
C(15)	0.3894(4)	0.918(1)	0.1927(5)	6.8(4)
C(16)	0.1310(5)	0.607(1)	−0.0155(4)	5.4(3)
C(17)	0.1605(4)	0.720(1)	−0.0232(3)	4.8(3)
C(18)	0.1847(5)	0.752(1)	−0.0566(4)	6.0(4)
C(19)	0.1954(4)	0.902(1)	−0.0033(4)	4.6(3)
C(20)	0.2376(5)	0.942(1)	−0.0696(5)	7.6(4)
C(21)	0.0512(4)	0.705(1)	−0.0193(4)	5.3(3)
C(22)	0.0251(4)	0.784(1)	0.0103(4)	4.5(3)
C(23)	−0.0212(4)	0.815(1)	0.0093(4)	5.1(3)
C(24)	0.0255(4)	0.908(1)	0.0692(4)	4.4(3)
C(25)	−0.0629(4)	0.948(1)	0.0600(5)	6.4(4)
C(26)	0.1727(4)	1.0127(10)	0.1062(3)	4.0(3)
C(27)	0.1868(5)	1.087(1)	0.1513(4)	5.5(3)
C(28)	0.1408(4)	1.094(1)	0.0683(4)	4.9(3)
C(29)	0.501(1)	0.077(3)	0.183(1)	22(1)

[a] $B_{eq} = 8\pi^2/3(U_{11}(aa^*)^2 + U_{22}(bb^*)^2 + U_{33}(cc^*)^2 + 2U_{12}aa^*bb^* \cos\gamma + 2U_{13}aa^*cc^* \cos\beta + 2U_{23}bb^*cc^* \cos\alpha)$.

Synthesis of Dicopper Complexes. The copper(II) complexes $[Cu_2(MeO)(mbipl)](ClO_4)_2$ (**1**) and $[Cu_2(MeO)(pbipl)](ClO_4)_2$ (**4**) were prepared from a ligand (Hmbipl·6HCl or Hpbipl·6HCl) and $Cu(ClO_4)_2$·$6H_2O$ in MeOH. Polymer formation was not observed using the present ligands even at high pH.

The methoxide bridge of **1** is easily exchanged by the other

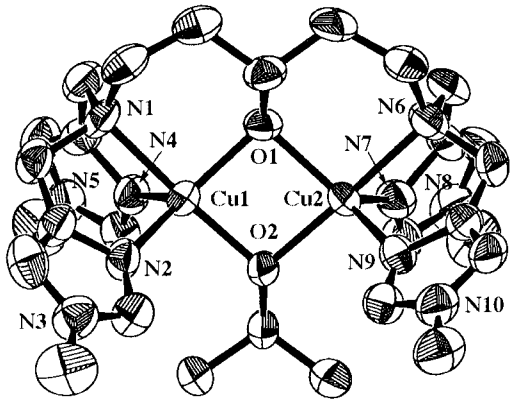

Figure 1. ORTEP view of the cation of **3**·CH_2Cl_2 with the atom-numbering scheme. The 50% probability thermal ellipsoids are shown. Hydrogen atoms have been omitted.

Scheme 1

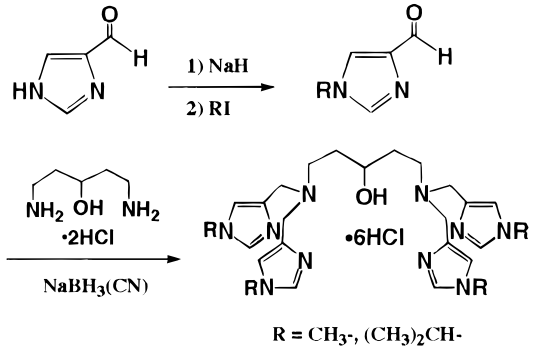

alcohols. The recystallization of **1** from EtOH−MeCN resulted in the isolation of $[Cu_2(EtO)(mbipl)](ClO_4)_2$ (**2**). The ligand exchange of **1** with 2-PrOH gave $[Cu_2(2\text{-}PrO)(mbipl)](ClO_4)_2$ (**3**). The easy exchange of the exogenous alkoxide bridge was also observed in the FAB mass spectra of the present complexes. The bridging alkoxide was exchanged with the matrix alcohol, *m*-nitrobenzyl alcohol (NBA). All fragment peaks as well as the parent peaks of the FAB mass spectra of **1**−**3** in the NBA matrix appear at identical positions while the intensities of these peaks are different each other. The parent peaks for **1**−**3** (*m*/*z* 870) and **4** (*m*/*z* 982) are assigned to $[M - ClO_4 - (\text{exogenous alkoxide}) + NBA]^+$. No peak assignable to complex cations having methoxide, ethoxide, or 2-propoxide bridge is observed. These results clearly demonstrate that the exogenous alkoxide bridges of the present complexes are exchanged with NBA under the FAB mass conditions. It is noteworthy that the intensity of the mass signals increases in the order **1**, **4** < **2** < **3**. This order seems to be the order of the easiness of the exchange of the exogenous alkoxide bridge. The dicopper complexes of Hmbipl and Hpbipl are more soluble in organic solvents than that of Hbipl. This is an advantage of the present complexes for acting as functional models of tyrosinase. The solubilities of the present complexes are different from each other; **4** is soluble in CH_2Cl_2, but **1** needs the aid of MeCN to dissolve in CH_2Cl_2. This indicates that the *N*-isopropyl groups increase the lipophilicity of **4**. These characteristics such as easy ligand exchange and high solubility in organic solvents are advantageous for modeling the function of tyrosinase.

Crystal Structures. The crystals of **2**·2MeCN and **3**·CH_2Cl_2 consist of a discrete dinuclear complex cation, two perchlorate ions, and crystal solvents. The ORTEP diagram of **3** is shown in Figure 1. The selected interatomic distances and the angles with their estimated standard deviations of **3** are given in Table 3. ORTEP diagrams of **2** are entered in the Supporting Information.

Table 3. Selected Bond Distances (Å) and Angles (deg) for $[Cu_2(2\text{-}PrO)(mbipl)](ClO_4)_2 \cdot CH_2Cl_2$ (**3**·CH_2Cl_2)

Bond Distances

Cu···Cu	2.926(2)				
Cu(1)−O(1)	1.969(6)	Cu(1)−O(2)	1.928(6)	Cu(1)−N(1)	2.092(8)
Cu(1)−N(2)	2.039(8)	Cu(1)−N(4)	2.225(8)	Cu(2)−O(1)	2.000(6)
Cu(2)−O(2)	1.927(6)	Cu(2)−N(6)	2.105(8)	Cu(2)−N(7)	2.101(9)
Cu(2)−N(9)	2.026(9)				

Bond Angles

Cu(1)−O(1)−Cu(2)	95.0(3)	Cu(1)−O(2)−Cu(2)	98.8(3)
O(1)−Cu(1)−O(2)	83.5(2)	O(1)−Cu(1)−N(1)	92.6(3)
O(1)−Cu(1)−N(2)	136.8(3)	O(1)−Cu(1)−N(4)	108.8(3)
O(2)−Cu(1)−N(1)	174.1(3)	O(2)−Cu(1)−N(2)	97.0(3)
O(2)−Cu(1)−N(4)	104.5 (3)	N(1)−Cu(1)−N(2)	82.8(3)
N(1)−Cu(1)−N(4)	80.9(3)	N(2)−Cu(1)−N(4)	112.8(3)
O(1)−Cu(2)−O(2)	82.7(2)	O(1)−Cu(2)−N(6)	94.2(3)
O(1)−Cu(2)−N(7)	112.5(3)	O(1)−Cu(2)−N(9)	129.4(3)
O(2)−Cu(2)−N(6)	172.6(3)	O(2)−Cu(2)−N(7)	105.8(3)
O(2)−Cu(2)−N(9)	95.9(3)	N(6)−Cu(2)−N(7)	81.5(3)
N(6)−Cu(2)−N(9)	80.8(4)	N(7)−Cu(2)−N(9)	116.3(3)

The copper coordination structures of **2** and **3** are similar to each other. Each cupric ion is pentacoordinate and is bound to two imidazole nitrogen atoms, a tertiary amine nitrogen atom, an endogenous bridging alkoxide oxygen atom, and an exogenous bridging alkoxide oxygen atom. The geometry around each Cu(II) ion can be described as a distorted trigonal bipyramid with the exogenous bridging alkoxide oxygen atom and the tertiay amine nitrogen atom occupying the axial position of each trigonal bipyramid. The degree of the distortion is estimated with the deviation from the expected 180° in the bond angles of O(2)−Cu(1)−N(1) and O(2)−Cu(2)−N(6) which are along the axis of the trigonal bipyramid. The deviations for the O(2)−Cu(1)−N(1) and O(2)−Cu(2)−N(6) angles are 6.4(3) and 5.9(3)° in **2** and 5.9(3) and 7.4(3)° in **3**, respectively. The degree of the distortion is also estimated with the deviation in the equatorial plane of the trigonal bipyramid. The largest deviations from the expected 120° are observed for the O(1)−Cu(1)−N(2) and O(1)−Cu(2)−N(9) angles, and these values are 13.4(3) and 13.8(3)° in **2** and 16.8(3) and 9.4(3)° in **3**, respectively. The degree of the distortion is estimated by the differences between two angles, (O(2)−Cu(1)−N(1)) − (O(1)−Cu(1)−N(2)) = 40.2° and (O(2)−Cu(2)−N(6)) − (O(1)−Cu(2)−N(9)) = 40.3° for **2** and 37.3 and 43.2° for **3**, respectively. These values vary from 0°, for an idealized square pyramid, to 60°, for an idealized trigonal bipyramid.[25] These data indicate that the copper coordination geometry in **2** and **3** consists of distorted trigonal bipyramids. Preliminary X-ray analysis of **4** shows that the copper coordination geometry in **4** is almost intermediate between a trigonal bipyramid and a square pyramid. Thus, the coordination geometry in **4** is the most distorted in **2**−**4**.

The Cu−O and Cu−N bond distances in **2** and **3** are typical of other copper(II) complexes. The distances for the Cu−O (exogenous alkoxide) bonds are shorter than those for the Cu−O (endogenous alkoxide) bonds. This is reasonable because the distance for a Cu−O (secondary alkoxide) bond is usually longer than that for a Cu−O (primary alkoxide) bond. The Cu−O (exogenous alkoxide) bond distances of **2** and **3** are different from each other. The value depends on the difference in the bulkiness of the exogenous alkoxide bridge. The distances for the Cu−O (exogenous alkoxide) bonds are 1.903(3) and 1.910(6) Å for **2** (ethoxide) and 1.927(6) and 1.928(6) Å for **3** (2-propoxide). This order corresponds to the ease of ligand exchange. The reverse tendency is observed in the Cu(1)−O(2)−Cu(2) bond angles, which are 99.6(3) and 98.8(3)° for **2** and **3**, respectively.

(25) Addison, A. W.; Rao, T. N. *J. Chem. Soc., Dalton Trans.* **1984**, 1349.

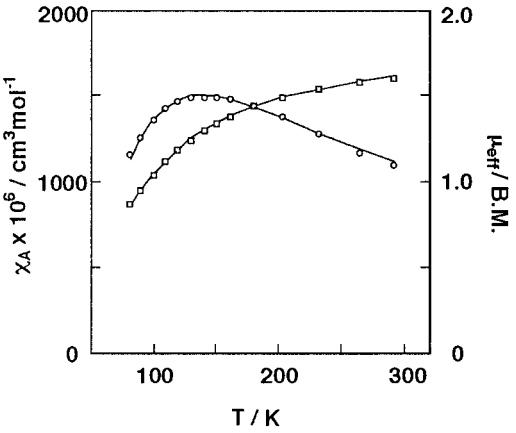

Figure 2. Temperature dependences of χ_A (○) and μ_{eff} (□) of **2**·2MeCN. Solid curves are based on eq 1, using $J = -77.05$ cm^{-1}, $g = 2.06$, and $N\alpha = 60$.

Table 4. Magnetic Susceptibility Parameters

compd	J/cm^{-1}	g	$N\alpha$	P/%
2·2MeCN	−77.05	2.06	60	0
3·CH_2Cl_2	−73.90	2.04	60	0
4·MeOH·CH_2Cl_2	−117.40	2.04	60	4

The Cu(1)−Cu(2) separations of **2** and **3** are 2.912(2) and 2.926(2) Å, respectively. These distances are approximately 0.1 Å shorter than the length reported for the (μ-methoxo)-dicopper(II) complex of 2,6-bis[(bis((1-methylimidazol-2-yl)-methyl)amino)methyl]-4-methylphenol (**6**).[16f] The Cu(1)−O(1)−Cu(2) bond angles (93.5−95.0°) in **2** and **3** are smaller than the corresponding bond angle (98.7°) in the phenoxide-bridged complex **6**. This is reasonably explained by the fact that six-membered chelate rings in **2** and **3** are composed of sp^3-carbon atoms but those in the endogenous phenoxide-bridged complex **6** contain two sp^2-carbon atoms. The small Cu−O−Cu bond angle reduces the Cu−Cu separation. The Cu−Cu separation of **3** is slightly larger than that of **2**. The bulkiness of 2-propoxide in **3** may expand the pocket surrounded by the four imidazole groups, increasing the Cu−Cu separation.

There is no interaction among any components in the cystal packing of **2** and **3**.

Magnetic Properties of 2−4. Magnetic susceptibility measurements of **2**−**4** were made on the crystals in the temperature range 80−300 K. The temperature dependence of the magnetic susceptibility (χ_A) and effective magnetic momemt (μ_{eff}) per Cu for **2** is shown in Figure 2. This shows a moderately strong antiferromagnetic exchange interaction between a pair of Cu(II) ions. The cryomagnetic properties of **3** and **4** are almost the same as that of **2** (see Supporting Information). The temperature dependence of χ_A for **2**−**4** is simulated by the modified Bleaney−Bowers equation including a correction term for paramagnetic impurities:

$$\chi_A = (Ng^2\beta^2/kT)[3 + \exp(-2J/kT)]^{-1}(1 - P)(0.45P/T) + N\alpha \quad (1)$$

Here P is the fraction of the monomeric copper(II) impurity and the other symbols have the usual meanings. An excellent fit of the χ_A-T data to the simulation was obtained when $J = -77.05$ cm^{-1}, $g = 2.06$, $N\alpha = 60$, and $P = 0$ were assumed for **2**. This simulation supports the X-ray analysis of **2**, where two MeCN molecules are included as crystal solvents. Similarly, good simulations have been attained for **3** and **4**. The best-fitting parameters obtained for these compounds are summarized in Table 4.

The coordination geometry about each copper ion in the three compounds is approximately trigonal bipyramidal, which leads to a d_{z^2} ground state. The major lobes of the d_{z^2} orbitals (magnetic orbitals) are oriented along the axial direction of the trigonal bipyramid toward the bridging exogenous alkoxide ligand. The two magnetic orbitals interact each other *via* a superexchange interaction through a p orbital of the exogenous alkoxide oxygen. The strength of the exchange interaction depends on the overlap of the three orbitals. Thus, the shorter Cu−O(2) bond and larger Cu(1)−O(2)−Cu(2) angle provide a better pathway for the antiferromagnetic interaction. In this study, the order of the strength of the exchange interaction is **4** > **2** > **3**, which is consistently explained by the Cu−O(2) bond lengths and the Cu(1)−O(2)−Cu(2) angles of **2** and **3** (see the description of the crystal structures). The antiferromagnetic interactions in **2**−**4** are stronger than that ($J = -47$ cm^{-1}) in the endogenous phenoxide- and exogenous methoxide-bridged dicopper complex **6**. The relatively strong antiferromagnetic interactions in **2**−**4** may be due to their shorter Cu−Cu separation compared with **6** (see the description of the crystal structures).

Physicochemical Properties. The electronic absorption spectra of compounds **1**−**4** in MeCN show distinct maxima between 200 and 900 nm. The ligand $\pi-\pi^*$ transitions occur around 210 nm for both Hmbipl and Hpbipl. The bands around 270 and 375 (sh) nm are assigned to the alcoholate−Cu(II) ligand-to-metal charge transfer (LMCT) transitions. The absorption coefficients of the LMCT bands at about 270 nm for the methoxodicopper complexes **1** (6770 M^{-1} cm^{-1}) and **4** (6370 M^{-1} cm^{-1}) are larger than those for the ethoxo- and 2-propoxodicopper complexes **2** (5930 M^{-1} cm^{-1}) and **3** (6190 M^{-1} cm^{-1}), suggesting that the overlap between the p-orbital of the exogenous alkoxide oxygen atom and the d_{z^2} orbitals of the copper atom in **1** and **4** is larger than that in **2** and **3**. In the case of **1**−**3**, the d−d transitions appear as broad bands at almost the same position, the data for λ_{max}/nm (ϵ/M^{-1} cm^{-1}) being 878 (226), 876 (225), and 875 (208) for **1**, **2**, and **3**, respectively. These broad and relatively low-energy d−d bands suggest that the trigonal bipyramidal geometry is kept in solution. In the case of **4**, the absorption peak of the d−d transition bands is shifted to 862 nm ($\epsilon = 228$ M^{-1} cm^{-1}). The blue-shift by ca. 15 nm suggests that the copper coordination geometry in **4** is slightly different from those in **1**−**3** and more distorted toward the square pyramidal one.

The cyclic voltammograms (CV) of **2**−**4** in MeCN are similar each other (see Supporting Information). The CV of **2** shows irreversible waves at $E_{pc} = -0.19$ and -0.32 and $E_{pa} = -0.10$ V vs Ag/Ag$^+$ leading to the Cu^{I}Cu^{II} and Cu^{I}Cu^{I} species, respectively. The CV of **3** is almost the same as that of **2**. This is consistently explained by the structural similarity between **2** and **3**, which is demonstrated by X-ray analyses and electronic absorption spectra. In the case of **4**, two cathodic waves and a broad anodic wave are observed. The cathodic peaks of **4** are shifted to -0.15 and -0.27 V vs Ag/Ag$^+$, and the anodic peak appears at the same potential as that of **2** and **3**. The positive shifts by 40−50 mV indicate that **4** is a better electron acceptor compared with **2** and **3**. This may be due to the relatively large distortion of the copper coordination geometry in **4**.

Catalytic Activity of Dicopper Complexes in the Oxidation of DBP. When an excess amount of DBP was added to a solution of **1**−**4** in MeCN, the green solution immediately turned yellow. The yellow solutions obtained from **1**−**3** show new absorption bands at about 325 nm (sh) and 425 nm (ϵ = ca. 2000 M^{-1} cm^{-1}) and d−d transition bands at 710 nm (ϵ = ca. 200 M^{-1} cm^{-1}). The color change is due to the appearance of the large absorption bands at about 325 and 425 nm, which are assignable to phenolate−Cu(II) LMCT bands, indicating an exchange of the exogenous alkoxide with phenoxide. The

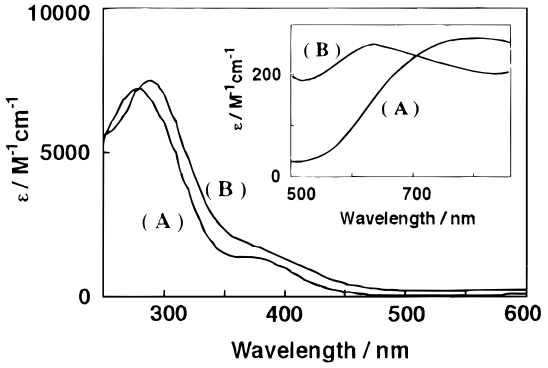

Figure 3. Electronic absorption spectra of (A) **4** and (B) a dicopper hydroperoxo complex **5** in CH_2Cl_2 containing less than 10% (v/v) MeCN at −30 °C.

intensity of the band at 425 nm increased with increasing concentration of DBP. At a low concentration of DBP, the compound for which exchange of the exogenous ligand is most facile gives the largest intensity band at 425 nm. The order of the intensity is **1** < **2** < **3**. At a high concentration of DBP, the extinction coefficients at 425 nm (LMCT bands) are saturated at ca. 2000 M^{-1} cm^{-1}. In the case of **4**, the apparent extinction coefficient at 417 nm (LMCT band) is saturated to show 1330 M^{-1} cm^{-1} by the addition of a 50-times excess amount of DBP. These data suggest that the exchange of the methoxide bridge in **4** is incomplete even at high concentration of DBP or that the LMCT band of the DBP complex generated from **4** is inherently weaker than that of the DBP complex generated from **1**−**3**. It seems that the bulky *N*-isopropyl groups in **4** make coordination of the sterically hindered DBP difficult. The role of the bulky *N*-alkyl groups is interesting from the mechanistic viewpoint and will be discussed later. The DBP complexes generated from **1**−**4** are quite stable under air at room temperature.

The yellow solution of the DBP complex in MeCN immediately turned green upon addition of aqueous H_2O_2 (30%). This color change is due to the disappearance of the phenolate−Cu(II) LMCT bands, indicating that DBP is replaced by H_2O_2 or water. The color change was observed in a mixed-solvent system (MeCN/CH_2Cl_2) as well as in MeCN when the aqueous H_2O_2 was added, but it was not observed in the mixed-solvent system when water was added in place of the aqueous H_2O_2, indicating that DBP is replaced by H_2O_2 in the mixed-solvent system to generate a hydroperoxodicopper(II) complex **5**.

Compound **5** is quite stable at temperatures below −40 °C, but it gradually decomposes to a structurally unkown blue complex at higher temperatures. Compound **5** shows absorption maxima at 290 (ϵ = 7520 M^{-1} cm^{-1}) and 642 nm (ϵ = ca. 250 M^{-1} cm^{-1}) (see Figure 3). These data are different from the absorption maxima reported for a hydroperoxodicopper(II) complex of 2,6-bis[bis((2-pyridylethyl)amino)methyl]phenoxide, 395 nm (ϵ = 8000 M^{-1} cm^{-1}) and 620 nm (ϵ = 450 M^{-1} cm^{-1}).[9b,26] This may be due to the difference in the endogenous bridging ligands, the alkoxide in this study and the phenoxide in the reported one.[9b,26] Similarly, hydroperoxodicopper(II) complexes were generated from **1**−**3** in the same manner.

Since compounds **1**−**3** are sparingly soluble in CH_2Cl_2, the mixed-solvent system (MeCN/CH_2Cl_2; see Experimental Section) was used in the catalytic oxidation of DBP. The green solution of the hydroperoxodicopper(II) complex turned brown in a few minutes in the presence of DBP at room temperature. The resultant reaction mixture was analyzed by GLC. The sole

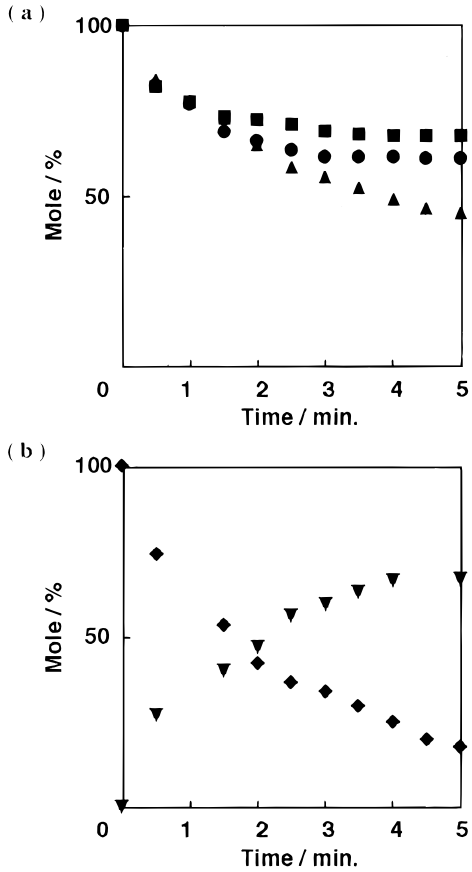

Figure 4. (a) Time course of decrease of DBP in the reaction catalyzed by **1**−**3**: **1** (●); **2** (▲); and **3** (■). (b) Time course of decrease (◆) of DBP and increase (▼) of product, 3,3′,5,5′-tetra-*tert*-butyl-2,2′-dihydroxybiphenyl, in the reaction catalyzed by **4**.

detectable product was 3,3′,5,5′-tetra-*tert*-butyl-2,2′-dihydroxybiphenyl. The time courses for the decrease of DBP in the reactions catalyzed by **1**−**3** are shown in Figure 4a. The decrease of DBP and the increase of the product in the reaction catalyzed by **4** are shown in Figure 4b. In the absence of the catalyst, the oxidation of DBP with aqueous H_2O_2 is very slow, the consumption of DBP being less than 5% after 1 day. It is certain, therefore, that **1**−**4** catalyze the oxidation of DBP efficiently.

The pseudo-first-order plots for the decrease of DBP in the oxidation catalyzed by **1**−**3** showed straight lines within the initial reaction (ca. 30% consumption of DBP) and provided almost the same rate constants, k_{obs} = ca. 4 × 10^{-3} s^{-1}. The reaction catalyzed by **1**−**3** was stopped at the stage of 40−60% consumption of DBP (see Figure 4a). This may be due to the decomposition of the catalyst. After the reaction, an aqueous blue-green solution was separated from the reaction mixture and was concentrated to give a blue-green solid which is insoluble in CH_2Cl_2. The FAB mass spectrum of the solid shows a parent peak at *m*/*z* 715 which is assignable to [{Cu_2(bipl)} + NBA − H]$^+$. The solid was treated with aqueous HCl to give an HCl salt of the ligand. The ^{1}H NMR spectrum of the isolated ligand did not show methyl signal. These results demonstrate that **1**−**3** are decomposed to [Cu_2(OR)(bipl)]$^{2+}$ during the reaction *via* an oxidative demethylation of mbipl. Since the complex [Cu_2(OR)(bipl)]$^{2+}$ thus formed is soluble in water, it transfers to an aqueous layer in the reaction mixture, resulting in the separation from DBP in organic layer. This may be the reason for the incomplete consumption of DBP in the reactions catalyzed by **1**−**3**.

On the other hand, DBP was consumed completely when **4** was used as a catalyst (see Figure 4b). This indicates that **4** is

(26) Karlin, K. D.; Ghosh, P.; Cruse, R. W.; Farooq, A.; Gultneh, Y.; Jacobson, R. R.; Blackburn, N. J.; Strange, R. W.; Zubieta, J. *J. Am. Chem. Soc.* **1988**, *110*, 6769.

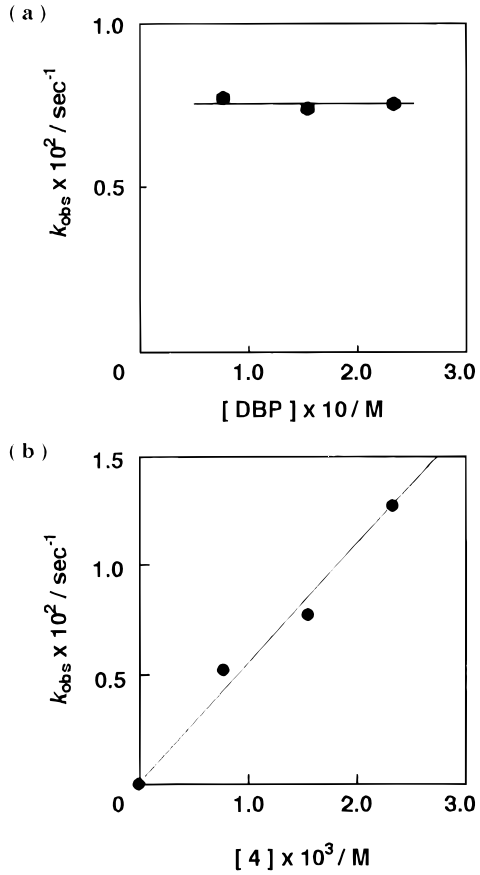

Figure 5. (a) Dependence of pseudo-first-order rate constants for the decrease of DBP on the concentration of DBP. [DBP] = (0.78−2.34) × 10^{-1} M, [**4**] = 1.56 × 10^{-3} M, H_2O_2 = 0.05 mL (30% in aqueous solution), and CH_2Cl_2/MeCN = 3 mL/0.2 mL, under air, at 25 ± 1 °C. (b) Dependence of pseudo-first-order rate constants for the decrease of DBP on the concentration of **4**. [**4**] = (0−2.34) × 10^{-3} M, [DBP] = 1.56 × 10^{-1} M, H_2O_2 = 0.05 mL (30% in aqueous solution), and CH_2Cl_2/MeCN = 3 mL/0.2 mL, under air, at 25 ± 1 °C.

more stable against the oxidation than **1**−**3**. The *N*-isopropyl groups on the imidazole rings may prevent the decomposition of **4**. The pseudo-first-order rate constant, 8 × 10^{-3} s^{-1}, in the DBP oxidation catalyzed by **4** is two times larger than those by **1**−**3** under the same conditions. The DBP oxidation may be accelerated by the relatively large distortion of the copper coordination geometry in **4**. Another reason for the acceleration by **4** is that the steric hindrance of the isopropyl groups in **4** prevents the formation of DBP complex and thus the hydroperoxodicopper complex is formed more easily from **4** than from **1**−**3**. Therefore, it is concluded that the bulky *N*-isopropyl groups enhance the catalytic activity of **4** through both accelerating the DBP oxidation and preventing the decomposition of **4**.

In order to clarify the reaction mechanism of the DBP oxidation, further kinetic studies have been carried out with **4**. The dependence of the pseudo-first-order rate constants on the concentrations of both **4** and DBP is shown in Figure 5. These data show that the DBP oxidation is first order with respect to both DBP and **4**. Thus, the rate equation of the reaction can be described as follows:

$$-\mathrm{d[DBP]}/\mathrm{d}t = k_2[\mathrm{DBP}][\mathbf{4}] \qquad (2)$$

Scheme 2

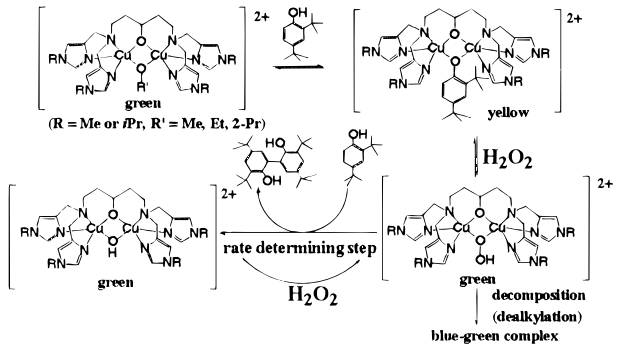

From this equation, the second-order rate constant, k_2, is calculated to be 5.3 M^{-1} s^{-1}.

A possible reaction mechanism deduced from the spectral and kinetic studies is shown in Scheme 2. Kinetic studies show that the transition state of the rate-determining step involves each one molecule of DBP and the catalyst. Since the DBP oxidation occurs after the formation of the hydroperoxodicopper complex, the rate-determining step might be the reaction of DBP with the hydroperoxodicopper complex.

Conclusion

Dicopper complexes with new tetraimidazole heptadentate ligands Hmbipl and Hpbipl have been synthesized and structurally characterized. The pendant imidazole nitrogens of the ligands are substituted by alkyl groups (methyl and isopropyl). Compounds **1**−**4** catalyze the oxidative coupling of DBP with H_2O_2. In the catalytic cycle, the hydroperoxodicopper(II) complex is formed as an active intermediate *via* an exchange of the exogenous bridging ligand with H_2O_2. The catalytic activity of **4** is enhanced by the bulky *N*-isopropyl groups around the active site. In general, bulky substituents are used to stabilize thermally unstable compounds by lowering the reactivities.[27] In this study, however, the bulky *N*-isopropyl groups of Hpbipl rather enhance the catalytic activity of its dicopper complex **4**.

Acknowledgment. We are grateful to Professor M. Mikuriya at Kwansei Gakuin University for kindly allowing us to use a Shimadzu UV-3100 spectrophotometer.

Supporting Information Available: Text giving details of the X-ray structural analyses and tables listing crystal structure refinement details, atomic coordinates, isotropic and anisotropic thermal parameters, bond distances and angles, and dihedral angles between planes of the trigonal bipyramid for the X-ray structure analyses of **2**·2MeCN and **3**·CH_2Cl_2, stereoviews and full cell diagrams, an ORTEP diagram of **2**, figures showing temperature dependences of the magnetic susceptibilities and the effective magnetic moments for **3** and **4**, and cyclic voltammograms for **2**−**4** (82 pages). X-ray crystallographic files, in CIF format, for compounds **2**·2MeCN and **3**·CH_2Cl_2 are available on the Internet only. Access and ordering information is given on any current masthead page.

IC961267V

(27) (a) Collman, J. P.; Gagne, R. R.; Reed, C. A.; Halbert, T. R.; Lang. G.; Robinson, W. T. *J. Am. Chem. Soc.* **1975**, *97*, 1427. (b) Harata, M.; Jitsukawa, K.; Masuda, H.; Einaga, H. *J. Am. Chem. Soc.* **1994**, *116*, 10817. (c) Cook, B. R.; Reinert, J.; Suslick, K. S. *J. Am. Chem. Soc.* **1986**, *108*, 7281.